Dynamical spontaneous scalarization in Einstein-Maxwell-scalar models in anti–de Sitter spacetime

Wen-Kun Luo,[1,*] Cheng-Yong Zhang,[1,†] Peng Liu,[1,‡] Chao Niu,[1,§] and Bin Wang[2,3,‖]

[1]*Department of Physics and Siyuan Laboratory, Jinan University, Guangzhou 510632, China*
[2]*Center for Gravitation and Cosmology, College of Physical Science and Technology, Yangzhou University, Yangzhou 225009, China*
[3]*School of Aeronautics and Astronautics, Shanghai Jiao Tong University, Shanghai 200240, China*

(Received 27 June 2022; revised 30 August 2022; accepted 8 September 2022; published 19 September 2022)

We study the dynamical spontaneous scalarization of charged black hole in asymptotically anti–de Sitter spacetimes in Einstein-Maxwell-scalar models. Including various nonminimal couplings between the scalar field and Maxwell field, an initial scalar-free black hole suffers tachyonic instability, and both the scalar field and the black hole irreducible mass grow exponentially at early times and saturate exponentially at late times. For fractional coupling, we find that, though there is negative energy distribution near the horizon, the black hole horizon area never decreases during the evolution. But when the parameters are large, the evolution end points of linearly unstable bald black holes will be spacetimes with a naked singularity such that the cosmic censorship is violated. The effects of the black hole charge, cosmological constant, and coupling strength on the dynamical scalarization process are studied in detail. We find that a large enough cosmological constant can prevent spontaneous scalarization.

DOI: 10.1103/PhysRevD.106.064036

I. INTRODUCTION

Black hole (BH) physics has been an intriguing subject for decades. Recently, high-precision observations have further stimulated interest to study this topic [1,2]. After the detection of gravitational waves from BH binary mergers [3–5] and the observation of a BH shadow by the Event Horizon Telescope [6–9], we have more new windows to disclose deep physics in BHs and examine the validity of general relativity (GR). In GR, there is a no-hair theorem in BH physics, which claims that, except the mass M, charge Q, and angular momentum J, there is no extra information we can learn from BHs [10–12]. But the no-hair theorem encounters challenges. Violations were observed in many gravity theories which allow hairy BH solutions, such as those with a Yang-Mills field [13–16], Skyrme field [17,18], conformally coupled scalar field [19], and the dilaton [20–22].

In addition to finding new hairy BH solutions to violate the no-hair theorem, it is of great interest to examine whether there are some relations between the no-hair BHs and hairy BHs, especially whether there is a mechanism to allow a transition between them. Recently, a peculiar dynamical mechanism, spontaneous scalarization, generating the hairy BHs has been revived. This mechanism was first found in the study of neutron stars in scalar-tensor theory [23–25]. A black hole in this theory can also be spontaneously scalarized if it is surrounded by a sufficient amount of matter [26–28]. BH spontaneous scalarization is triggered by the tachyonic instability of the scalar field, through the nonminimal coupling between the scalar field ϕ and a source term I. The backreaction of the scalar instability can destroy the bald BH and lead to the formation of a stable scalarized BH. The source term I can be the Gauss-Bonnet invariant [29–32], Ricci scalar for nonconformally invariant black holes [33], Chern-Simons invariant [34], or Maxwell invariant, etc. [35]. Recent studies of BH spontaneous scalarization arose in the extended scalar-tensor Gauss-Bonnet (eSTGB) theory [36–44]. However, the equations of motion in the eSTGB theory are difficult to solve because of the challenging ill-posedness problem [45–49], so that many works limit their dynamical studies in the decoupling limit [50–54]. The Einstein-Maxwell-scalar (EMS) theory is considered as a technically simpler model and has attracted much attention in examining the dynamics of scalarization, without losing the general interest [55–61].

Considering the special asymptotic boundary in anti–de Sitter (AdS) spacetime, which behaves as a reflection mirror, it is intriguing to examine whether there are some special properties of spontaneous scalarization in AdS spacetime [62–64]. We will reveal the influence of the negative cosmological constant together on the dynamical

*luowk@stu2020.jnu.edu.cn
†zhangcy@email.jnu.edu.cn
‡phylp@email.jnu.edu.cn
§niuchaophy@gmail.com
‖wang_b@sjtu.edu.cn

spontaneous scalarization in detail. This can help to have a further insight into the special properties of the scalarization in AdS spacetime. On the other hand, it is known that the properties of the scalarized BH depend heavily on the coupling function and the appropriate ranges of parameters in the system [30–32]. In this work, we will carefully investigate dynamical BH spontaneous scalarization in EMS models with various coupling functions in asymptotically AdS spacetimes and uncover quantitatively the dependence of the dynamical process on the coupling strength between the scalar field and electromagnetic field.

Especially, for the EMS model with a fractional coupling function, the phase diagrams disclosed in Ref. [55] are very different with other couplings. The end point of the instability of the RN-AdS BH in the region where the charge to mass ratio and coupling parameter are large is an open question and needs further studies from dynamical simulation. We will show that in this parameter region cosmic censorship is violated during the evolution and the end point should be a spacetime with a naked singularity. Cosmic censorship has been tested in EMS theory [65], in which the authors found that naked singularities do not form for a power coupling function. In eSTGB theory, cosmic censorship has also been tested very recently [66,67]. The authors simulated the mass loss due to evaporation at the classical level using an auxiliary phantom field and suggested that either weak cosmic censorship is violated or horizonless remnants are produced. Here, we find that, without introducing an exotic phantom field, cosmic censorship can also be violated.

This work is organized as follows. In Sec. II, we discuss the general framework, introduce the source terms in the EMS theory, and write out the equations of motion in the Eddington-Finkelstein coordinate. In Sec. III, we give the conditions generating spontaneous scalarization, the choices of coupling functions, and the boundary conditions of AdS spacetime. The numerical results are presented in Sec. IV. Finally, we summarize and discuss the results obtained.

II. MODEL SETUP

A. The action and equations of motion

The action we consider in this work is

$$S = -\frac{1}{16\pi}\int d^4x\sqrt{-g}[R - 2\Lambda - 2\partial_\mu\phi\partial^\mu\phi - f_i(\phi)I(\psi;g)]. \tag{1}$$

Here, R is the Ricci scalar, and $\Lambda = -3/L^2$ is the cosmological constant with the AdS radius L. The scalar field ϕ is minimally coupled to the metric $g_{\mu\nu}$ and nonminimally coupled to the source term $I(\psi, g)$, which generically depends on the spacetime metric $g_{\mu\nu}$ and the extra matter fields, collectively denoted by ψ. The subscript i in coupling function $f_i(\phi)$ will be used to label the various coupling choices. In EMS theory, the extra matter field is a gauge field A_μ with

$$I(\psi, g) = F_{\mu\nu}F^{\mu\nu} \tag{2}$$

in which $F_{\mu\nu} = \partial_\mu A_\nu - \partial_\nu A_\mu$ is the electromagnetic field strength tensor. In eSTGB theory, the source term is Gauss-Bonnet invariant $I(\psi; g) = R^2 - 4R_{\mu\nu}R^{\mu\nu} + R_{\mu\nu\rho\sigma}R^{\mu\nu\rho\sigma}$ and $\psi = 0$, i.e., without any extra matter fields.

The field equations obtained by varying the action with respect to $g_{\mu\nu}$, ϕ, and A_μ are

$$R_{\mu\nu} - \frac{1}{2}Rg_{\mu\nu} + \Lambda g_{\mu\nu} = 2\bigg[\partial_\mu\phi\partial_\nu\phi - \frac{1}{2}g_{\mu\nu}\partial_\rho\phi\partial^\rho\phi + f(\phi)\bigg(F_{\mu\rho}F_\nu{}^\rho - \frac{1}{4}g_{\mu\nu}F_{\rho\sigma}F^{\rho\sigma}\bigg)\bigg], \tag{3}$$

$$\frac{1}{\sqrt{-g}}\partial_\mu(\sqrt{-g}\partial^\mu\phi) = \frac{1}{4}\frac{df(\phi)}{d\phi}F_{\rho\sigma}F^{\rho\sigma}, \tag{4}$$

$$\partial_\mu(\sqrt{-g}f(\phi)F^{\mu\nu}) = 0. \tag{5}$$

B. Conditions for spontaneous scalarization of black holes

We assume that the model admits scalar-free solutions, i.e., $\phi = 0$ satisfies the equations of motion (3)–(5). The coupling function $f(\phi)$ must obey the following criteria.

(i) $f(\phi)|_{\phi=0,r\to\infty} = 1$.—The system approaches the electromagnetic vacuum in the far region.
(ii) $\frac{df(\phi)}{d\phi}|_{\phi=0} = 0$.—This allows the existence of a scalar-free solution.
(iii) $\frac{d^2f(\phi)}{d\phi^2}|_{\phi=0} > 0$.—This guarantees the appearance of the tachyonic instability which drives the system away from the scalar-free solution.

In fact, to guarantee the existence of nontrivial scalarized BHs, one can also derive the constraints equivalent to conditions (i) and (iii) from Eq. (4) in the case of purely electric (or magnetic) RN BHs, which is the so-called Bekenstein-type inequality $f(\phi)_{,\phi\phi} > 0$ and $\phi f_{,\phi} > 0$ [58].

C. Selection of coupling function

In this work, we simulate the dynamical evolution of the BH spontaneous scalarization in EMS theory in AdS spacetime with coupling functions satisfying the above conditions, which include

(i) a fractional coupling $f_F(\phi) = \frac{1}{1+b\phi^2}$;
(ii) a hyperbolic cosine coupling $f_H(\phi) = \cosh(\sqrt{-2b}\phi)$; and
(iii) a power coupling $f_P(\phi) = 1 - b\phi^2$.

The parameter b is a dimensionless constant in all cases. The couplings f_H and f_P were widely studied in the context of holographic superfluid and superconductor [68]. The coupling f_F was used to study the phase transitions near black hole horizons [69]. It gives analytical spontaneously scalarized black hole solutions [35,70,71]. When b is negative enough, all these three couplings can trigger the spontaneous scalarization and have been studied in many recent works [35,55,58,60,70–72]. However, these works did not examine the dynamics in detail. Especially, the end point of the unstable bald black hole with a large charge to mass ratio in the EMS model with fractional coupling function f_F is unclear. We choose these three coupling functions to clarify these interesting issues and explore whether there are qualitatively different behaviors in the dynamical spontaneous scalarization.

Hereafter, we consider $b < 0$. We emphasize that these three coupling functions have the same leading-order expansion $1 - b\phi^2$ for small ϕ. Since the tachyonic instability of the initial bald black hole is determined by the quadratic term, they have almost the same existence lines in the domains of existence of scalarized BHs in asymptotically flat spacetime, as shown in Fig. 3 in Ref. [55]. However, the critical sets of domains of existence of scalarized BHs are significantly different. This implies the higher-order terms in the coupling function expansion have strong influence on the properties of the scalarized BHs. Note that, for fractional coupling $f_F = \frac{1}{1+b\phi^2}$, the expansion near $\phi = 0$ cannot be continued to $|\phi| > \frac{1}{\sqrt{-b}}$. It diverges at $|\phi| = \frac{1}{\sqrt{-b}}$ and becomes negative when $|\phi| > \frac{1}{\sqrt{-b}}$. This will lead to qualitatively different properties of the scalarized BH and the dynamics, such as negative energy density and violation of cosmic censorship.

III. NUMERICAL SETUP

A. Equations of motion in Eddington-Finkelstein coordinate

We study the dynamical formation of a charged scalarized BH from a spherically symmetric scalar-free RN-AdS BH suffering tachyonic instability in EMS theory, by adopting the ingoing Eddington-Finkelstein coordinate ansatz

$$ds^2 = -\alpha(t,r)dt^2 + 2dtdr + \zeta(t,r)^2(d\theta^2 + \sin^2\theta d\varphi^2). \quad (6)$$

Here, $\alpha(t,r)$ and $\zeta(t,r)$ are the metric functions. They are regular on the BH apparent horizon which satisfies $g^{\mu\nu}\partial_\mu\zeta\partial_\nu\zeta = 0$. We choose the gauge field as

$$A_\mu dx^\mu = A(t,r)dt. \quad (7)$$

Plugging the above ansatz into Eq. (5) yields the first integral

$$\partial_r A = \frac{Q}{\zeta^2 f(\phi)}, \quad (8)$$

in which Q is an integral constant interpreted as the electric charge of the BH. To implement the numerical method, we introduce auxiliary variables

$$S = \partial_t\zeta + \frac{1}{2}\alpha\partial_r\zeta. \quad (9)$$

$$P = \partial_t\phi + \frac{1}{2}\alpha\partial_r\phi. \quad (10)$$

Substituting these into Eq. (3), we get

$$\partial_t S = \frac{1}{2}S\partial_r\alpha + \frac{\alpha}{2}\left(\frac{2S\partial_r\zeta - 1}{2\zeta} + \frac{1}{2}\zeta\Lambda + \frac{Q^2}{2\zeta^3 f(\phi)}\right) - \zeta P^2, \quad (11)$$

$$\partial_r^2\alpha = -4P\partial_r\phi + \frac{4S\partial_r\zeta - 2}{\zeta^2} + \frac{4Q^2}{\zeta^4 f(\phi)}, \quad (12)$$

$$\partial_r S = \frac{1 - 2S\partial_r\zeta}{2\zeta} - \frac{\zeta\Lambda}{2} - \frac{Q^2}{2\zeta^3 f(\phi)}, \quad (13)$$

$$\partial_r^2\zeta = -\zeta(\partial_r\phi)^2. \quad (14)$$

The scalar equation (4) gives

$$\partial_r P = -\frac{P\partial_r\zeta + S\partial_r\phi}{\zeta} - \frac{Q^2}{4\zeta^4 f(\phi)^2}\frac{df(\phi)}{d\phi}. \quad (15)$$

As long as the initial ϕ is given, we can integrate constraint equations (12)–(15) to get initial α, S, ζ, and P. The ϕ on the next time slice can be obtained from the evolution equation (10). This formulation has been widely used to simulate the nonlinear dynamics in AdS spacetimes due to its simplicity and high accuracy [63,64,73–79].

B. Boundary conditions of AdS spacetime

To solve the set of differential equations numerically, we have to implement suitable boundary conditions. An asymptotic approximation of the variables in the far region takes the form

$$\phi = \frac{\phi_3(t)}{r^3} + \frac{3}{8\Lambda r^4}(-bQ^2 - 8\phi_3'(t)) + O(r^{-5}), \quad (16)$$

$$\alpha = -\frac{\Lambda}{3}r^2 + 1 - \frac{2M}{r} + \frac{Q^2}{r^2} + \frac{\Lambda}{5r^4}\phi_3^2(t) + O(r^{-5}), \quad (17)$$

$$\zeta = r - \frac{3\phi_3^2(t)}{10r^5} + \frac{3\phi_3(t)}{14\Lambda r^6}(-bQ^2 - 8\phi_3'(t)) + O(r^{-7}), \quad (18)$$

$$S = -\frac{\Lambda}{6}r^2 + \frac{1}{2} - \frac{M}{r} + \frac{Q^2}{2r^2} - \frac{3\Lambda}{20r^4}\phi_3^2(t) + O(r^{-5}), \quad (19)$$

$$P = \frac{\Lambda\phi_3(t)}{2r^2} + \frac{1}{r^3}\left(\frac{-bQ^2}{4} - \phi_3'(t)\right) + \frac{3}{2\Lambda r^4}\phi_3''(t) + O(r^{-5}), \tag{20}$$

in which $\phi_3'(t) = \frac{d\phi_3(t)}{dt}$. This series expansion contains three constants: the Arnowitt-Deser-Misner (ADM) mass M, the charge Q of the BH, and the cosmological constant Λ. Hereafter, we fix the value of the ADM mass as $M = 1$ in this work to implement the dimensionless of the physical quantities. Meanwhile, we study the BH irreducible mass M_{ir} and the rescaled Misner-Sharp mass M_{ms}, which are, respectively, defined as

$$M_{\mathrm{ir}} = \sqrt{\frac{A_H}{4\pi}} = \zeta(t, r_H), \tag{21}$$

$$M_{\mathrm{ms}} = \frac{m}{4\pi} = \frac{1}{2}\zeta\left(1 - \frac{\Lambda}{3}\zeta^2 - g^{\mu\nu}\partial_\mu\zeta\partial_\nu\zeta\right). \tag{22}$$

Here, $A_H = 4\pi\zeta^2(t, r_H)$ and r_H stands for the coordinate location of the BH apparent horizon. The irreducible mass equals the horizon area radius. At the static case, ϕ_3 can be viewed as the scalar charge indicating the existence of scalar hair. But it is unknown here and needs to determined by evolution. Notice that some of the variables in the series expansion above like α, ζ, and S are divergent at infinity. Therefore, the following new variables are introduced for numerical calculation:

$$\zeta \equiv r\sigma, \qquad \alpha \equiv r^2 a, \qquad S \equiv r^2 s, \qquad P \equiv \frac{1}{r}p. \tag{23}$$

In addition, the scalar perturbation in AdS spacetime can reach spatial infinity at a finite coordinate time and be bounced back to the bulk. So spatial infinity must be included in the computational domain. The effective way is to compact the radial direction by a coordinate transformation, i.e., $z = \frac{r}{r+M}$. In this new coordinate, the computational domain that we take is $(z_i, 1)$, where z_i is close to but smaller than the initial BH apparent horizon and $z = 1$ corresponds to spatial infinity. From the above conditions, we can obtain the boundary conditions at infinity:

$$\begin{aligned} &\sigma = 1, \qquad \sigma' = 0, \qquad s = -\frac{\Lambda}{6}, \qquad s' = 0, \\ &s'' = 6(M-1), \qquad p = 0, \\ &a = -\frac{\Lambda}{3}, \qquad a' = 0, \qquad a'' = 12(M-1). \end{aligned} \tag{24}$$

Here, the prime denotes the derivative with respect to z. For the initial profiles of the scalar field, we take the Gaussian wave packet

$$\phi_0 = ae^{-(\frac{r-cM}{wM})^2}. \tag{25}$$

Here, a, c, and w parametrize the initial amplitude, center, and width of the Gaussian wave, respectively.

IV. NUMERICAL RESULTS

In this section, we will show that for all three coupling functions considered here, in the parameter region where the bald RN-AdS BH and scalarized BH coexist, the RN-AdS BH suffers tachyonic instability and evolves into a scalarized BH. The dynamical behaviors are qualitatively similar to those found in the EMS model with exponential coupling function $f_E(\phi) = e^{-b\phi^2}$ [63]. The scalar field grows exponentially at early times and saturates to a final value at late times. However, as shown in Fig. 3 in Ref. [55], the domain of existence of scalarized BHs in EMS models with fractional coupling f_F in asymptotically flat spacetime is rather different from those with hyperbolic cosine or power couplings. Especially when both the charge to mass ratio Q/M and $-b$ are large, the bald BH still suffers tachyonic instability, but the end point of the instability is unclear. Here, we will show that, in asymptotically AdS spacetime, the end point of tachyonic instability of a RN-AdS BH with large Q/M and $-b$ should be a spacetime with a naked singularity. Note that tachyonic instability happens near the horizon so that the qualitative behaviors will not be changed by the AdS boundary at spatial infinity. So we can conclude that, in asymptotically flat spacetime, the end point of the RN BH with large Q/M in the EMS model with fractional coupling should also be a spacetime with a naked singularity.

A. Results for fractional coupling

1. Scalar field for fractional coupling $f_F(\phi)$

We first investigate the final spatial distribution of the scalar field when the system reaches equilibrium starting from an unstable RN-AdS BH with a fractional coupling function under initial scalar perturbation. As shown in Fig. 1, an obvious feature is that the scalar field piles up at the horizon. It is nodeless and monotonically tends to zero in all situations. The final scalar field value on the BH horizon grows with Q and $-b$ while decreasing with Λ. Note that the coupling function f_F is negative near the horizon and positive in the far region. It diverges at $\phi = -\frac{1}{\sqrt{-b}}$ at a certain radius. However, this divergence is benign, since the coupling function always appears in combinations $\frac{1}{f_F(\phi)} = 1 + b\phi^2$ and $\frac{1}{f_F(\phi)^2}\frac{df_F(\phi)}{d\phi} = -2b\phi$ for fractional coupling in the equations in Sec. III A. So the geometry and the scalar field are smooth therein.

To figure out how the system evolves from the initial bald RN-AdS BH to the final hairy BH, we show the evolution of the scalar field value on the horizon ϕ_H in the upper row in Fig. 2. One can find that the BH is decorated with scalar hair faster and more heavily for larger Q and

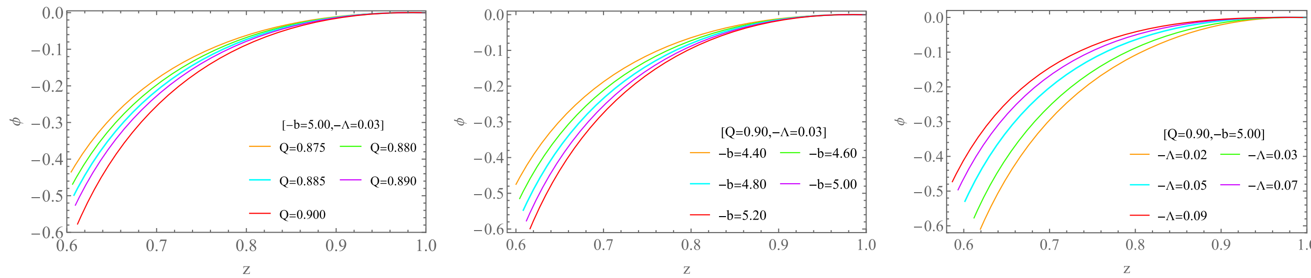

FIG. 1. The spatial distribution of the scalar field ϕ outside the horizon for various charge Q, coupling constant b, and cosmological constant Λ when the system reaches equilibrium.

stronger coupling $-b$ between the scalar field and Maxwell field. On the contrary, the cosmological constant Λ suppresses this phenomenon. These are consistent with the results from Fig. 1.

In the middle and lower rows in Fig. 2, we show the evolution of $\log|\phi_H(f) - \phi_H(t)|$ and $\log|\phi_H(t) - \phi_H(i)|$. Here, $\phi_H(i) = 0$ and $\phi_H(f)$ are the initial and final scalar field value on the horizon, respectively. The lower row implies that, if the RN-AdS BH is in the unstable regime, any initial arbitrarily small perturbation will result in an exponential growth of the scalar field at early times. The middle row implies that the scalar field saturates to an equilibrium value at late times and the final equilibrium BH is endowed with scalar hair. Hence, the evolution of the scalar field on the horizon can be approximated by

$$\phi_H \approx \begin{cases} \exp(\nu_i t + \nu_1), & \text{early times}, \\ \phi_H(f) - \exp(-\nu_f t + \nu_2), & \text{late times}. \end{cases} \tag{26}$$

Here, ν_i is the growth rate of ϕ_H at early times, and ν_f is the imaginary part of dominant mode frequency at late times. $\nu_{1,2}$ are some subdominant terms depending on Q, b, and Λ. The lower row in Fig. 2 reveals that ν_i is positively related to Q and $-b$ and negatively related to $-\Lambda$, which means that the time of a scalarized BH bifurcating from the initial RN-AdS BH will be shortened during the growth stage for larger Q and $-b$ and prolonged for larger $-\Lambda$. At late times, however, the central row in Fig. 2 shows that, during the saturation stage, ϕ_H takes a longer time to converge to its final value for larger Q and $-b$ and smaller $-\Lambda$. On the other hand, the relations between ν_f and Q, b, and Λ are contrary to those of ν_i.

2. *Misner-Sharp mass of fractional coupling*

The Misner-Sharp mass M_{ms} of scalarized solutions is a function of the radius and time. Its final distribution when the system reaches equilibrium is exhibited in the upper

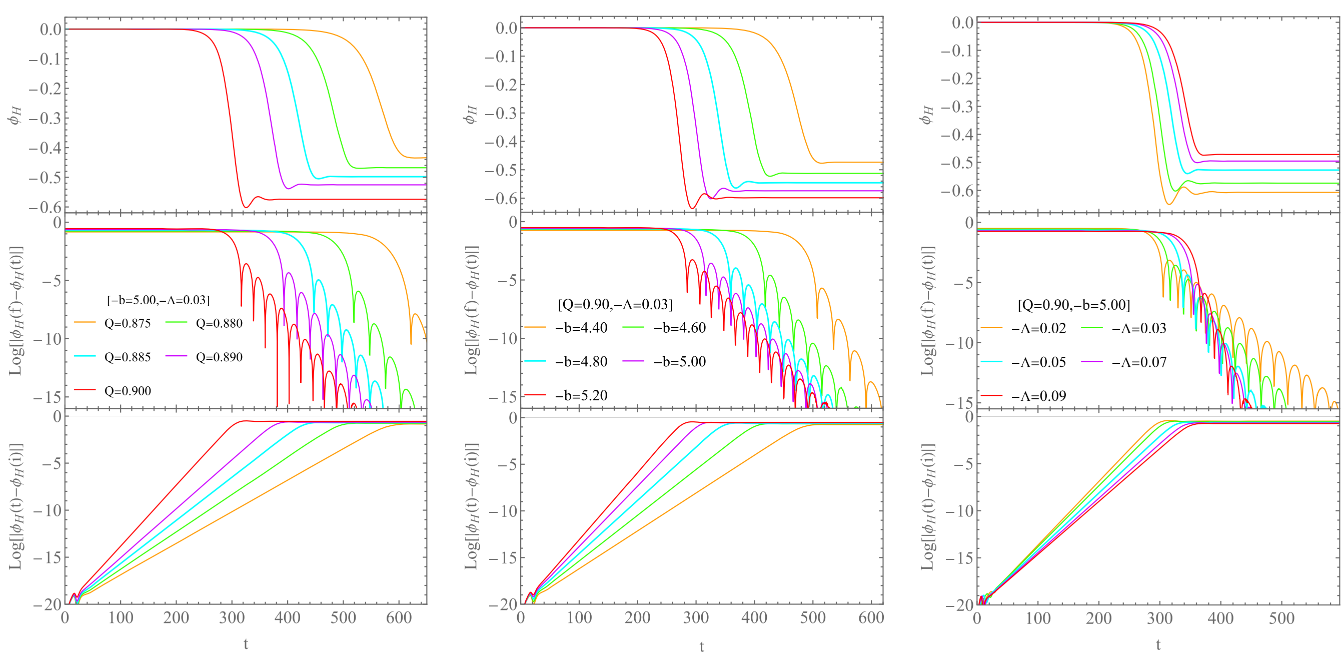

FIG. 2. The upper row shows the evolution of the scalar field value ϕ_H on the horizon. The lower and center rows indicate that ϕ_H grows exponentially at first and then saturates to an equilibrium value with damped oscillation.

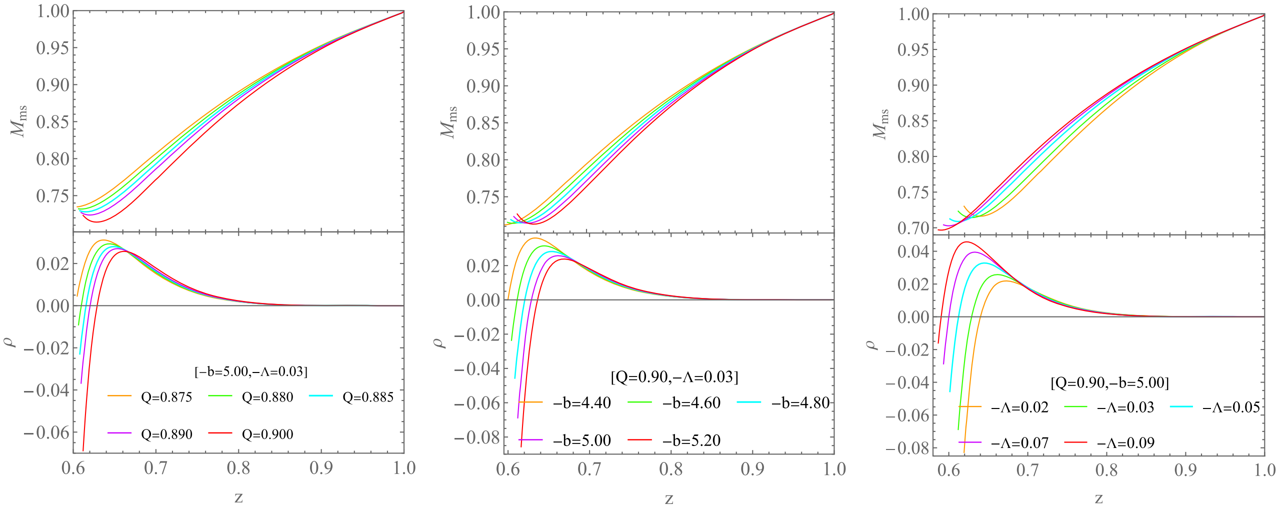

FIG. 3. Fractional coupled scalarized BH solutions exhibit negative energy densities ρ in the vicinity of the horizon. Note that the left end points locate on the BH horizon, and we show only the distribution outside the horizon.

row in Fig. 3. It increases to the ADM mass $M = 1$ as the radius tends to infinity. However, in the near horizon region, the $M_{\rm ms}$ decreases with radius for large Q and $-b$ and small $-\Lambda$. This implies that there is negative energy distribution near the black hole. In fact, for a static solution, the energy density can be expressed as

$$\rho = \frac{\alpha}{2}\left(\frac{\partial\phi}{\partial r}\right)^2 + \frac{Q^2}{2\zeta^4 f(\phi)} = \frac{\alpha}{2}\left(\frac{\partial\phi}{\partial r}\right)^2 + \frac{Q^2(1+b\phi^2)}{2\zeta^4}, \tag{27}$$

which follows from $\rho = T_{\mu\nu}Z^\mu Z^\nu$. Here, $T_{\mu\nu}$ is the stress energy tensor in Eq. (3), and $Z^\mu = (\partial_t)^\mu/\sqrt{\alpha}$. The energy density distribution is shown in the lower row in Fig. 3. One can find that the scalarized BH solution obtained with fractional coupling does have negative energy density in the vicinity of the horizon. This is similar to the results found in asymptotically flat spacetime [55]. Actually, the negative energy originates from the second term in Eq. (27), since $1 + b\phi^2 < 0$ in the vicinity of the horizon. The negative contribution is more significant for stronger coupling and larger charge.

The extremum of ρ and the negative energy band Δz are shown in Fig. 4. The $\rho(\min)$ decreases monotonically with Q or $-b$, while Δz first remains zero and then increases. This result can also be explained by Eq. (27), in which the first term is always positive outside the horizon. For small Q or $-b$, the final scalarized BH has less hair so that the first term is larger than the second term, so the energy density ρ is positive and the negative energy band Δz is zero. On the one hand, the right row in Fig. 4 shows that the increase of $-\Lambda$ suppresses the negative energy distribution outside the horizon.

3. Naked singularity

The above subsection shows that the negative energy becomes more significant for stronger coupling parameter $-b$. Here, we show that $-b$ cannot be too large; otherwise, a naked singularity will appear inevitably. The left panel in Fig. 5 shows the evolution of the Ricci scalar for $Q = 0.9$, $-\Lambda = 0.03$, and $-b = 20$. The Ricci scalar explodes in the interior of the apparent horizon. Although our code crashes at late times, we suggest that the curvature singularity moves outward rapidly and finally passes through the

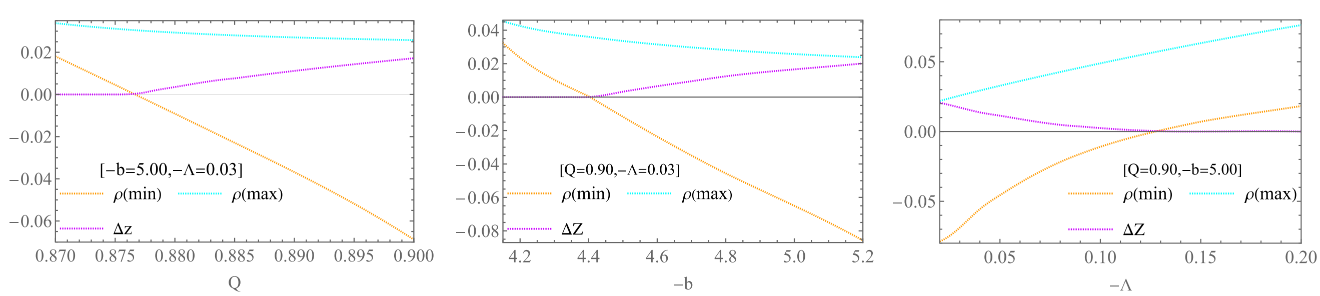

FIG. 4. The maximum and minimum of the energy density ρ outside the horizon, the negative energy band Δz, and the minimum of the Misner-Sharp mass versus Q, b, and Λ.

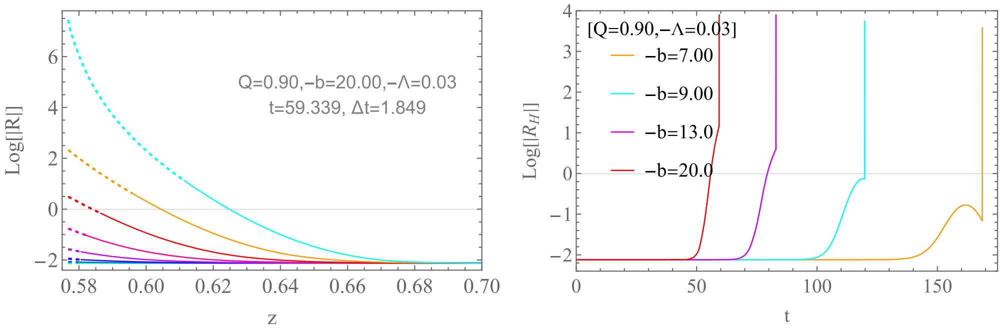

FIG. 5. Left: the evolution of scalar curvature R when $Q = 0.9$, $-\Lambda = 0.03$, and $-b = 20$. The time step between adjacent curves is $\Delta t = 1.8546$. The uppermost curve corresponds to $t = 59.3390$, after which our code crashes soon. The dashed parts represent the results in the interior of the apparent horizon. Right: the evolution of scalar curvature on the apparent horizon R_H for various b when $Q = 0.9$ and $-\Lambda = 0.03$ before our code crashes.

apparent horizon such that a naked singularity forms. From another viewpoint, we show the evolution of the scalar curvature on the apparent horizon R_H in the right panel. The R_H also explodes with time. For larger $-b$, the R_H increases faster and our code crashes earlier. We conclude that, for large $-b$, the evolution end point of a linearly unstable RN-AdS black hole is a spacetime with a naked singularity such that weak cosmic censorship is violated [80]. In eSTGB theory, cosmic censorship violation has also been suggested when they simulate the mass loss due to evaporation at the classical level using an exotic phantom field [66,67]. Here, we find that, without introducing the exotic phantom field, cosmic censorship can also be violated. In EMS theory with fractional coupling, the negative energy density and violation of cosmic censorship follows not from the presence of an exotic form of matter but from the synergy of the scalar field coupling with the Maxwell term.

4. Irreducible mass of fractional coupling

Figure 6 displays the evolution of the BH irreducible mass $M_{\rm ir}$ for various Q, $-b$, and $-\Lambda$. The irreducible mass equals the BH apparent horizon area radius. In the upper row, one can find that the irreducible mass never decreases during the evolution, although the weak energy condition is violated, as discussed in the above subsection. This is permissible, since the weak energy condition is a sufficient but not necessary condition for the black hole area increase law [81,82]. The nonlinear evolution exhibits no other obvious pathologies apart from the negative energy density. The scalarized solutions are both thermodynamically and dynamically preferred.

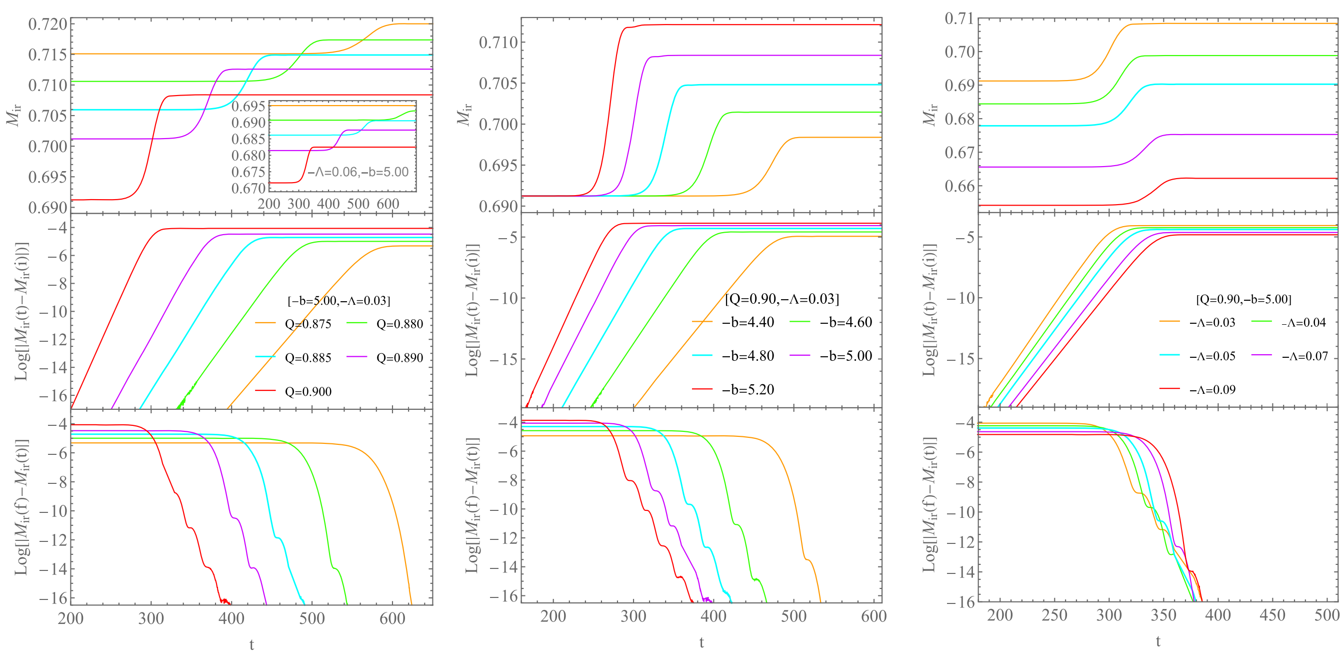

FIG. 6. The evolution of irreducible mass $M_{\rm ir}$ for various coupling constant b, charge Q, and cosmological constant Λ.

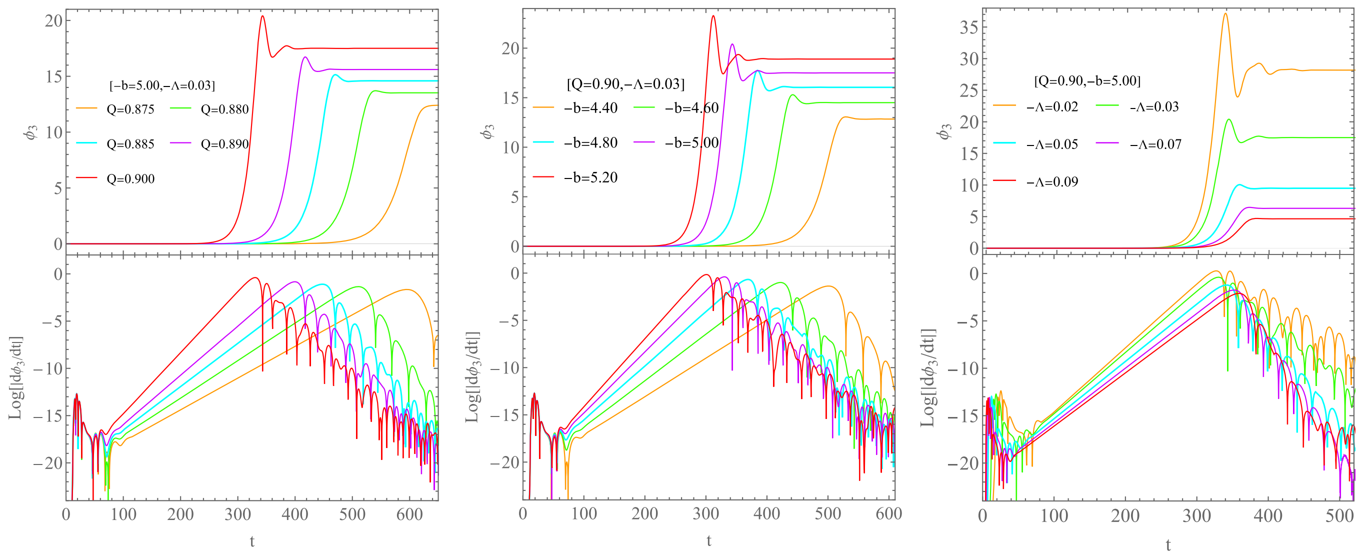

FIG. 7. The evolution of ϕ_3. It resembles the evolution of ϕ_H, although the sign is reversed (upper row). The lower row shows the evolution of $\log|\frac{d\phi_3}{dt}|$.

The irreducible mass increases with Q and $-b$. This can be understood from the coupling term between the Maxwell field and the scalar field in the action. For larger Q or $-b$, the coupling is stronger. More energy will be transferred from the Maxwell field to the scalar field. The BH can swallow more scalar field, and its area grows. The cosmological constant Λ, however, puts a more stringent condition for spontaneous scalarization. Comparing the evolution of M_{ir} at different Λ in the upper-left inset in Fig. 6, within certain parameter ranges, the original scalar-free BH is stabilized due to the increase of $-\Lambda$. In fact, in asymptotic AdS spacetime, the tachyonic instability occurs only when its effective mass squared is less than the Breitenlohner-Freedman bound $\mu^2_{\mathrm{BF}} = \frac{3\Lambda}{4}$ [62,63,83]. For large enough $-\Lambda$, the tachyonic instability can be quenched.

Another interesting feature is that the evolution of irreducible mass M_{ir} can be roughly divided into two stages. The center and lower rows in Fig. 6 illustrate that both the early stage and the late stages follow exponential evolution:

$$M_{\mathrm{ir}}(t) \approx \begin{cases} M_{\mathrm{ir}}(i) + \exp(\gamma_i t + \gamma_1), & \text{early times,} \\ M_{\mathrm{ir}}(f) - \exp(-\gamma_f t + \gamma_2), & \text{late times.} \end{cases} \tag{28}$$

Here, γ_i and γ_f are the exponential growth rate and saturation rate of M_{ir}, respectively. $M_{\mathrm{ir}}(i)$ and $M_{\mathrm{ir}}(f)$ are the initial and final irreducible mass of the BH, respectively. $\gamma_{1,2}$ are some terms less important. Note that $M_{\mathrm{ir}}(i)$ of the initial RN-AdS BH depends on Q and Λ. From the middle row in Fig. 6, the relationship between γ_i and Q, b, and Λ is analogous to those of the ϕ_H at the horizon. However, the saturation stage is stepped rather than damped oscillation, as shown in the lower row in Fig. 6.

5. ϕ_3 of fractional coupling

Now we investigative the evolution of coefficient ϕ_3 of the scalar field at spatial infinity. Figure 7 shows that the evolution of ϕ_3 resembles the evolution of ϕ_H, which can also be divided roughly into two stages. At early stage, it increases exponentially. At late time, it converges to the equilibrium value $\phi_3(f)$ with damped oscillation which resembles the quasinormal mode. Its evolution can be approximated by

$$\phi_3 \approx \begin{cases} \exp(\eta_i t + \eta_1), & \text{early times,} \\ \phi_3(f) - \exp(-\eta_f t + \eta_2), & \text{late times.} \end{cases} \tag{29}$$

Here, η_i is the growth rate of ϕ_3 at early times and η_f the imaginary part of the dominant mode frequency of ϕ_3 at late times. $\eta_{1,2}$ are some terms less important. The lower row in Fig. 7 shows that η_i is positively related to Q and $-b$ and negatively related to Λ. Meanwhile, η_f has contrary relations to Q, $-b$, and Λ.

There are universal and robust relationships between ϕ_H, M_{ir}, and ϕ_3 during the evolution:

$$\gamma_i = 2\nu_i = 2\eta_i, \qquad \gamma_f = 2\nu_f = 2\eta_f. \tag{30}$$

This relationship can be understood for an intermediate solution which can be approximated by a static solution. For a static solution, the variables S, α, and P are zero on the horizon. So combining Eqs. (9), (10), (11), (13), and (15) one can find $\partial_t S$, $\partial_t \zeta \propto \delta\phi^2$ for the intermediate solution. Since $S(r_H, t) = 0$ and Eq. (21) states that $M_{\mathrm{ir}} = \zeta(r_H, t)$, we can deduce that $\dot{M}_{\mathrm{ir}} = \dot{\zeta}(r_H, t) = -\frac{\partial_t S}{\partial_r S}\partial_r \zeta + \partial_t \zeta|_{r_H} \propto \dot{\phi}^2_H$. Since, at early and late times, the evolution can be approximated by the perturbations

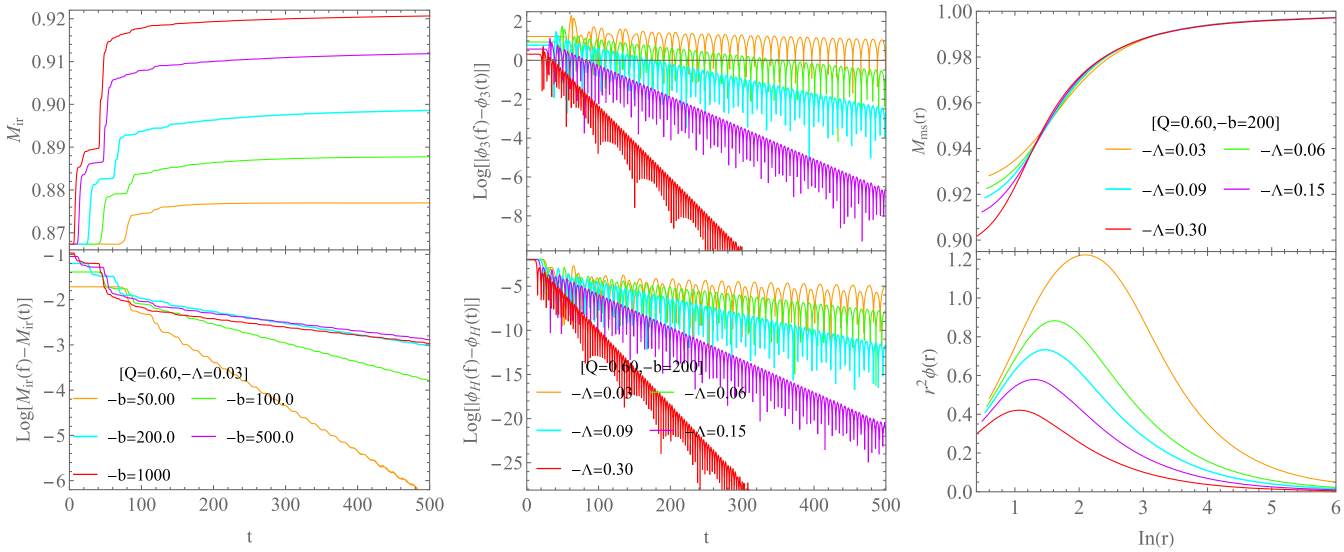

FIG. 8. Left column: the evolution of the irreducible mass $M_{\rm ir}$ for models with a hyperbolic coupling function. Middle column: the evolution of ϕ_3 and ϕ_H. Right column: the final profiles of the Misner-Sharp mass and $r^2\phi$ for different Λ.

for the initial and final BHs, respectively, this leads to the relations (30). These relations have been found in other cases [22,63,64,84].

B. Results for power-law and hyperbolic coupling

In this subsection, we consider the dynamics of the spontaneous scalarization with coupling functions $f_H = \cosh\sqrt{-2b}\phi$ and $f_P = 1 - b\phi^2$. The results for hyperbolic coupling are shown in Fig. 8. For the power coupling, the dynamical features are qualitatively similar. In fact, the dynamical features of the spontaneous scalarization for power and hyperbolic couplings in asymptotically AdS spacetime are qualitatively similar to those found in the model with coupling $f_E = \exp(-b\phi^2)$ which has been studied in Ref. [63]. For both f_H, f_P, and f_E, the evolution of M_{ir}, ϕ_H, and ϕ_3 still obeys the exponential growth at the early stage and exponentially saturates to the equilibrium value at late times. The spontaneous scalarization is enhanced by Q and $-b$ but suppressed by Λ. On the other hand, the final distribution of the Misner-Sharp mass monotonically increases to the ADM mass at spatial infinity. There is no negative energy distribution outside the BH horizon. This is very different than the case with f_F, in which negative energy appears near the horizon. This can be explained by Eq. (27) from which we see that the energy density can be negative for f_F only when $b < 0$.

V. CONCLUSION

We have focused attention on the dynamical spontaneous scalarization in the asymptotically AdS spacetime in EMS models. We have discussed three different coupling functions $f_F(\phi)$, $f_H(\phi)$, and $f_P(\phi)$. They have the same leading quadratic order expansion $1 - b\phi^2$ in the limit of a small scalar field with exponential coupling $f_E(\phi)$. Since the tachyonic instability which triggers the spontaneous scalarization is mainly determined by the quadratic term, the dynamical evolution features of $f_F(\phi)$, $f_H(\phi)$, and $f_P(\phi)$ are qualitatively similar to those with the exponential coupling $f_E(\phi)$ [63]. In the parameter region where the tachyonic instability is triggered, we found that a bald RN-AdS BH can be spontaneously transformed into a scalarized BH, which is also preferred in thermodynamics. We have explored the effects of the BH charge Q, coupling strength parameter b, and cosmological constant Λ on the dynamical process in the scalarization. When the system reaches equilibrium, the extreme value of ϕ always locates at the horizon (denoted as ϕ_H). Starting from the initial bald RN-AdS BH, we find that ϕ_H grows exponentially at the early stage of the dynamical evolution in the scalarization. At the late stage in the process of scalarization, ϕ_H converges to an equilibrium value through damped oscillation. We find that the scalarization is enhanced by larger values of Q and $-b$ but suppressed with the increase of Λ. We have also investigated the evolution of ϕ_3 and find that ϕ_3 evolves similarly to ϕ_H.

The irreducible mass $M_{\rm ir}$ never decreases during the dynamical spontaneous scalarization of the BH. Since $M_{\rm ir}$ is the horizon area radius and the BH entropy is proportional to the horizon area, this feature is a signal that the second law of thermodynamics is obeyed, although the weak energy condition is violated in models with a fractional coupling function. $M_{\rm ir}$ grows exponentially at early times and saturates also exponentially to the final value at late times. The corresponding growth coefficient γ_i and saturation coefficient γ_f increase with Q and $-b$. The increase of $\gamma_{i,f}$ can shorten the growth and saturation time of $M_{\rm ir}$. On the other hand, the cosmological constant plays a contrary role that prolongs the time for dynamical scalarization.

For the EMS model with fractional coupling, there is negative energy distribution near the BH horizon. The negative energy region is stretched with the increase of Q and $-b$ and narrowed with Λ. However, Q and $-b$ cannot be too large. Once these parameters reach maximum thresholds, a naked singularity will appear during the dynamical evolution and cosmic censorship is violated. Compared with fractional coupling $f_F(\phi)$, the cases with hyperbolic coupling $f_H(\phi)$, power coupling $f_P(\phi)$, and exponential coupling $f_E(\phi)$ in AdS spacetime do not have negative energy distribution. The difference comes from the fact that f_H, f_P, and f_E are always positive, since the spontaneous scalarization occurs only for negative b. However, the fractional coupling f_F can be negative in some space region such that the kinetic term of the Maxwell field has the "wrong sign" in the action. Note that the negative energy density and violation of cosmic censorship follow not from the presence of an exotic form of fundamental matter but from the synergy of the scalar field coupling with the Maxwell term. This is different from the violation of cosmic censorship induced by the exotic phantom field used in the study of eSTGB theory [66,67].

ACKNOWLEDGMENTS

This work is supported by the Natural Science Foundation of China under Grants No. 11805083, No. 11905083, No. 12005077, and No. 12075202 and Guangdong Basic and Applied Basic Research Foundation (2021A1515012374).

[1] E. Berti *et al.*, Testing general relativity with present and future astrophysical observations, Classical Quantum Gravity **32**, 243001 (2015).
[2] L. Barack *et al.*, Black holes, gravitational waves and fundamental physics: A roadmap, Classical Quantum Gravity **36**, 143001 (2019).
[3] B. P. Abbott *et al.*, Observation of Gravitational Waves from a Binary Black Hole Merger, Phys. Rev. Lett. **116**, 061102 (2016).
[4] B. P. Abbott *et al.*, GW170104: Observation of a 50-Solar-Mass Binary Black Hole Coalescence at Redshift 0.2, Phys. Rev. Lett. **118**, 221101 (2017).
[5] B. P. Abbott *et al.*, GWTC-1: A Gravitational-Wave Transient Catalog of Compact Binary Mergers Observed by LIGO and Virgo during the First and Second Observing Runs, Phys. Rev. X **9**, 031040 (2019).
[6] P. V. P. Cunha and C. A. R. Herdeiro, Shadows and strong gravitational lensing: A brief review, Gen. Relativ. Gravit. **50**, 42 (2018).
[7] K. Akiyama *et al.* (Event Horizon Telescope Collaboration), First M87 Event Horizon Telescope Results. I. The shadow of the supermassive black hole, Astrophys. J. **875**, L1 (2019).
[8] K. Akiyama *et al.* (Event Horizon Telescope Collaboration), First M87 Event Horizon Telescope Results. IV. Imaging the central supermassive black hole, Astrophys. J. Lett. **875**, L4 (2019).
[9] K. Akiyama *et al.* (Event Horizon Telescope Collaboration), First M87 Event Horizon Telescope Results. VI. The shadow and mass of the central black hole, Astrophys. J. Lett. **875**, L6 (2019).
[10] Werner Israel, Event horizons in static vacuum space-times, Phys. Rev. **164**, 1776 (1967).
[11] B. Carter, Axisymmetric Black Hole Has Only Two Degrees of Freedom, Phys. Rev. Lett. **26**, 331 (1971).
[12] P. T. Chrusciel, J. Lopes Costa, and M. Heusler, Stationary black holes: Uniqueness and beyond, Living Rev. Relativity **15**, 7 (2012).
[13] M. S. Volkov and D. V. Galtsov, Non-Abelian Einstein Yang-Mills black holes, JETP Lett. **50**, 346 (1989), http://jetpletters.ru/ps/1130/article_17118.shtml.
[14] P. Bizon, Colored Black Holes, Phys. Rev. Lett. **64**, 2844 (1990).
[15] B. R. Greene, S. D. Mathur, and C. M. O'Neill, Eluding the no hair conjecture: Black holes in spontaneously broken gauge theories, Phys. Rev. D **47**, 2242 (1993).
[16] K. I. Maeda, T. Tachizawa, T. Torii, and T. Maki, Stability of Non-Abelian Black Holes and Catastrophe Theory, Phys. Rev. Lett. **72**, 450 (1994).
[17] H. Luckock and I. Moss, Black holes have skyrmion hair, Phys. Lett. B **176**, 341 (1986).
[18] S. Droz, M. Heusler, and N. Straumanm, New black hole solutions with hair, Phys. Lett. B **268**, 371 (1991).
[19] J. D. Bekenstein, Exact solutions of Einstein conformal scalar equations, Ann. Phys. (N.Y.) **82**, 535 (1974).
[20] P. Kanti, N. E. Mavromatos, J. Rizos, K. Tamvakis, and E. Winstanley, Dilatonic black holes in higher curvature string gravity, Phys. Rev. D **54**, 5049 (1996).
[21] C. Y. Zhang, P. Liu, Y. Liu, C. Niu, and B. Wang, Evolution of Anti-de Sitter black holes in Einstein-Maxwell-dilaton theory, Phys. Rev. D **105**, 024010 (2022).
[22] C. Y. Zhang, P. Liu, Y. Liu, C. Niu, and B. Wang, Dynamical scalarization in Einstein-Maxwell-dillton theory, Phys. Rev. D **105**, 024073 (2022).
[23] T. Damour and G. Esposito-Farese, Nonperturbative Strong Field Effects in Tensor-Scalar Theories of Gravitation, Phys. Rev. Lett. **70**, 2220 (1993).
[24] T. Damour and G. Esposito-Farese, Tensor-scalar gravity and binary pulsar experiments, Phys. Rev. D **54**, 1474 (1996).

[25] T. Harada, Stability analysis of spherically symmetric star in scalar-tensor theories of gravity, Prog. Theor. Phys. **98**, 359 (1997).
[26] V. Cardoso, I. P. Carucci, P. Pani, and T. P. Sotiriou, Black Holes with Surrounding Matter in Scalar-Tensor Theories, Phys. Rev. Lett. **111**, 111101 (2013).
[27] V. Cardoso, I. P. Carucci, P. Pani, and T. P. Sotiriou, Matter around Kerr black holes in scalar-tensor theories: scalarization and superradiant instability, Phys. Rev. D **88**, 044056 (2013).
[28] C. Y. Zhang, S. J. Zhang, and B. Wang, Superradiant instability of Kerr-de Sitter black holes in scalar-tensor theory, J. High Energy Phys. 08 (2014) 011.
[29] G. Antoniou, A. Bakopoulos, and P. kanti, Evasion of No-Hair Theorems and Novel Black-Hole Solutions in Gauss-Bonnet Theories, Phys. Rev. Lett. **120**, 131102 (2018).
[30] D. D. Doneva and S. S. Yazadjiev, New Gauss-Bonnet Black Holes with Curvature-Induced Scalarization in Extended Scalar-Tensor Theories, Phys. Rev. Lett. **120**, 131103 (2018).
[31] H. O. Silva, J. Sakstein, L. Gualtieri, T. S. Sotiriou, and Emanuele, Spontaneous Scalarization of Black Holes and Compact Stars from a Gauss-Bonnet Coupling, Phys. Rev. Lett. **120**, 131104 (2018).
[32] J. L. Blázquez-Salcedo, D. D. Doneva, J. Kunz, and S. S. Yazadjiev, Radial perturbations of the scalarized Einstein-Gauss-Bonnet black holes, Phys. Rev. D **98**, 084011 (2018).
[33] C. A. R. Herdeiro and E. Radu, Black hole scalarisation from the breakdown of scale invariance, Phys. Rev. D **99**, 084039 (2019).
[34] Y. Brihaye, C. Herdeiro, and E. Radu, The scalarized Schwarzschild-NUT spacetime, Phys. Lett. B **788**, 295 (2019).
[35] C. A. R. Herdeiro, E. Radu, N. Sanchis-Gual, and J. A. Font, Spontaneous Scalarization of Charged Black Holes, Phys. Rev. Lett. **121**, 101102 (2018).
[36] G. Antoniou, A. Bakopoulos, and P. Kanti, Black-hole solutions with scalar hair in Einstein-scalar-Gauss-Bonnet theories, Phys. Rev. D **97**, 084037 (2018).
[37] Y. S. Myung and D. C. Zou, Gregory-Laflamme instability of black hole in Einstein-scalar-Gauss-Bonnet theories, Phys. Rev. D **98**, 024030 (2018).
[38] M. Minamitsuji and T. Ikeda, scalarized black holes in the presence of the coupling to Gauss-Bonnet gravity, Phys. Rev. D **99**, 044017 (2019).
[39] P. V. P. Cunha, C. A. R. Herdeiro, and E. Radu, Spontaneously Scalarized Kerr Black Holes in Extended-Scalar-Tensor-Gauss-Bonnet Gravity, Phys. Rev. Lett. **123**, 011101 (2019).
[40] C. F. B. Macedo, J. Sakstein, E. Berti, L. Gualtieri, H. O. Silva, and T. P. Sotiriou, Self-interactions and spontaneous black hole scalarization, Phys. Rev. D **99**, 104041 (2019).
[41] C. A. R. Herdeiro, E. Radu, H. O. Silva, T. P. Sotiriou, and N. Yunes, Spin-Induced Scalarized Black Holes, Phys. Rev. Lett. **126**, 011103 (2021).
[42] E. Berti, L. G. Collodel, B. Kleihaus, and J. Kunz, Spin-Induced Black-Hole Scalarization in Einstein-Scalar-Gauss-Bonnet Theory, Phys. Rev. Lett. **126**, 011104 (2021).
[43] A. Dima, E. Barausse, N. Franchini, and T. P. Sotiriou, Spin-Induced Black Hole Spontaneous Scalarization, Phys. Rev. Lett. **125**, 231101 (2020).
[44] A. Bakopoulos, G. Antoniou, and P. Kanti, Novel black-hole solutions in Einstein-scalar-Gauss-Bonnet theories with a cosmological constant, Phys. Rev. D **99**, 064003 (2019).
[45] J. L. Ripley and F. Pretorius, Hyperbolicity in spherical gravitational collapse in a Horndeski theory, Phys. Rev. D **99**, 084014 (2019).
[46] J. L. Ripley and F. Pretorius, Dynamics of a Z2 symmetric EdGB gravity in spherical symmetry, Classical Quantum Gravity **37**, 155003 (2020).
[47] W. E. East and J. L. Ripley, Evolution of Einstein-scalar-Gauss-Bonnet gravity using a modified harmonic formulation, Phys. Rev. D **103**, 044040 (2021).
[48] W. E. East and J. L. Ripley, Dynamics of Spontaneous Black Hole Scalarization and Mergers in Einstein-Scalar-Gauss-Bonnet Gravity, Phys. Rev. Lett. **127**, 101102 (2021).
[49] Y. Liu, C. Y. Zhang, W. L. Qian, K. Lin, and B. Wang, Dynamic generation or removal of a scalar hair, arXiv:2206.05012.
[50] D. D. Doneva and S. S. Yazadjiev, Dynamics of the non-rotating and rotating black hole scalarization, Phys. Rev. D **103**, 064024 (2021).
[51] H. J. Kuan, D. D. Doneva, and S. S. Yazadjiev, Dynamical Formation of Scalarized Black Holes and Neutron Stars through Stellar Core Collapse, Phys. Rev. Lett. **127**, 161103 (2021).
[52] D. D. Doneva and S. S. Yazadjiev, Beyond the spontaneous scalarization: New fully nonlinear mechanism for the formation of scalarized black holes and its dynamical development, Phys. Rev. D **105**, L041502 (2022).
[53] H. O. Silva, H. Witek, M. Elley, and N. Yunes, Dynamical Descalarization in Binary Black Hole Mergers, Phys. Rev. Lett. **127**, 031101 (2021).
[54] D. D. Doneva, A. Vañó-Viñuales, and S. S. Yazadjiev, Dynamical descalarization with a jump during black hole merger, arXiv:2204.05333.
[55] P. G. S. Fernandes, C. A. R. Herdeiro, A. M. Pombo, E. Radu, and N. Sanchis-Gual, Spontaneous scalarisation of charged black holes: Coupling dependence and dynamical features, Classical Quantum Gravity **36**, 134002 (2019).
[56] J. L. Blázquez-Salcedo, C. A. Herdeiro, J. Kunz, A. M. Pombo, and E. Radu, Einstein-Maxwell-scalar black holes: The hot, the cold and the bald, Phys. Lett. B **806**, 135493 (2020).
[57] Y. S. Myung and D. C. Zou, Instability of Reissner-Nordstr'om black hole in Einsten-Maxwell-scalar theory, Eur. Phys. J. Spec. Top. **79**, 273 (2019).
[58] D. Astefanesei, C. Herdeiro, and A. Pombo, Einstein-Maxwell-scalar black holes: Classes of solutions, dyons and extremality, J. High Energy Phys. 10 (2019) 078.
[59] Y. Brihave, C. Herdeiro, and E. Radu, Black hole spontaneous scalarisation with a positive cosmological constant, Phys. Lett. B **802**, 135269 (2020).
[60] P. G. S. Fernandes, C. A. R. Herdeiro, A. M. Pombo, E. Radu, and N. Sanchis-gual, Charged black holes with axionic-type couplings: Classes of solutions and dynamical scalarization, Phys. Rev. D **100**, 084045 (2019).

[61] W. Xiong, P. Liu, C. Niu, C. Y. Zhang, and B. Wang, Dynamical spontaneous scalarization in Einstein-Maxwell-scalar theory, Chin. Phys. C **46**, 095103 (2022).

[62] G. Guo, P. Wang, and H. Wu, Scalarized Einstein-Maxwell-scalar black holes in anti-de Sitter spacetime, Eur. Phys. J. C **81**, 864 (2021).

[63] C. Y. Zhang, P. Liu, Y. Liu, C. Niu, and B. Wang, Dynamical charged black hole spontaneous scalarisation in anti-de Sitter spacetimes, Phys. Rev. D **104**, 084089 (2021).

[64] C. Y. Zhang, Q. Chen, Y. Liu, W. K. Luo, Y. Tian, and B. Wang, Dynamical transitions in scalarization and descalarization through black hole accretion, arXiv:2204.09260.

[65] F. Corelli, T. Ikeda, and P. Pani, Challenging cosmic censorship in Einstein-Maxwell-scalar theory with numerically simulated gedanken experiments, Phys. Rev. D **104**, 084069 (2021).

[66] F. Corelli, M. De Amicis, T. Ikeda, and P. Pani, What is the fate of Hawking evaporation in gravity theories with higher curvature terms?, arXiv:2205.13006.

[67] F. Corelli, M. De Amicis, T. Ikeda, and P. Pani, Nonperturbative gedanken experiments in Einstein-dilaton-Gauss-Bonnet gravity: Nonlinear transitions and tests of the cosmic censorship beyond General Relativity, arXiv: 2205.13007.

[68] M. Cadoni, G. D'Appollonio, and P. Pani, Phase transitions between Reissner-Nordstrom and dilatonic black holes in 4D AdS spacetime, J. High Energy Phys. 03 (2010) 100.

[69] S. S. Gubser, Phase transitions near black hole horizons, Classical Quantum Gravity **22**, 5121 (2005).

[70] C. A. R. Herdeiro and J. M. S. Oliveira, Electromagnetic dual Einstein-Maxwell-scalar models, J. High Energy Phys. 07 (2020) 130.

[71] C. A. R. Herdeiro, T. Ikeda, M. Minamitsuji, T. Nakamura, and E. Radu, Spontaneous scalarization of a conducting sphere in Maxwell-scalar models, Phys. Rev. D **103**, 044019 (2021).

[72] R. A. Konoplya and A. Zhidenko, Analytical representation for metrics of scalarized Einstein-Maxwell black holes and their shadows, Phys. Rev. D **100**, 044015 (2019).

[73] P. M. Chesler and L. G. Yaffe, Horizon Formation and Far-From-Equilibrium Isotropization in Supersymmetric Yang-Mills Plasma, Phys. Rev. Lett. **102**, 211601 (2009).

[74] M. J. Bhaseen, J. P. Gauntlett, B. D. Simons, J. Sonner, and T. Wiseman, Holographic Superfluids and the Dynamics of Symmetry Breaking, Phys. Rev. Lett. **110**, 015301 (2013).

[75] P. M. Chesler and L. G. Yaffe, Numerical solution of gravitational dynamics in asymptotically anti-de Sitter spacetimes, J. High Energy Phys. 07 (2014) 086.

[76] R. A. Janik, J. Jankowski, and H. Soltanpanahi, Real-Time Dynamics and Phase Separation in a Holographic First Order Phase Transition, Phys. Rev. Lett. **119**, 261601 (2017).

[77] P. M. Chesler and D. A. Lowe, Nonlinear Evolution of the AdS4 Superradiant Instability, Phys. Rev. Lett. **122**, 181101 (2019).

[78] P. Bosch, S. R. Green, and L. Lehner, Nonlinear Evolution and Final Fate of Charged Anti-de Sitter Black Hole Superradiant Instability, Phys. Rev. Lett. **116**, 141102 (2016).

[79] P. Bosch, S. R. Green, L. Lehner, and H. Roussille, Excited hairy black holes: Dynamical construction and level transitions, Phys. Rev. D **102**, 044014 (2020).

[80] R. M. Wald, Gravitational collapse and cosmic censorship, in *Black Holes, Gravitational Radiation and the Universe* (Springer, Dordrecht, 1999).

[81] S. W. Hawking and G. F. R. Ellis, *The Large Scale Structure of Space-Time* (Cambridge University Press, Cambridge, England, 1973).

[82] A. B. Nielsen, Black holes and black hole thermodynamics without event horizons, Gen. Relativ. Gravit. **41**, 1539 (2009).

[83] P. Breitenlohner and D. Z. Freedman, Stability in gauged extended supergravity, Ann. Phys. (N.Y.) **144**, 249 (1982).

[84] C. Y. Zhang, Q. Chen, Y. Liu, W. K. Luo, Y. Tian, and B. Wang, Critical Phenomena in Dynamical Scalarization of Charged Black Hole, Phys. Rev. Lett. **128**, 161105 (2022).